Pre-Steady-State Kinetic Studies of the Fidelity and Mechanism of Polymerization Catalyzed by Truncated Human DNA Polymerase λ†

Kevin A. Fiala,‡,§,|| Wissam Abdel-Gawad,‡,§,⊥ and Zucai Suo*,§,||,⊥,#,△

Department of Biochemistry, Ohio State Biochemistry Program, Ohio State Biophysics Program, Molecular, Cellular, and Developmental Biology Program, and Comprehensive Cancer Center, The Ohio State University, Columbus, Ohio 43210

Received January 2, 2004; Revised Manuscript Received April 1, 2004

ABSTRACT: DNA polymerase λ (Polλ), a member of the X-family DNA polymerases, possesses an N-terminal BRCT domain, a proline-rich domain, and a C-terminal polymerase β-like domain (tPolλ). In this paper, we determined a minimal kinetic mechanism and the fidelity of tPolλ using pre-steady-state kinetic analysis of the incorporation of a single nucleotide into a one-nucleotide gapped DNA substrate, 21-19/41-mer (primer-primer/template). Our kinetic studies revealed an incoming nucleotide bound to the enzyme·DNA binary complex at a rate constant of 1.55×10^8 M^{-1} s^{-1} to form a ground-state ternary complex while the nucleotide dissociated from this complex at a rate constant of 300 s^{-1}. Since DNA dissociation from tPolλ (0.8 s^{-1}) was less than 3-fold slower than polymerization, we measured saturation kinetics for all 16 possible nucleotide incorporations under single turnover conditions to eliminate the complication resulting from multiple turnovers. The fidelity of tPolλ was estimated to be in the range of 10^{-2}−10^{-4} and was sequence-dependent. Surprisingly, the ground-state binding affinity of correct (1.1−2.4 μM) and incorrect nucleotides (1.4−8.4 μM) was very similar while correct nucleotides (3−6 s^{-1}) were incorporated much faster than incorrect nucleotides (0.001−0.2 s^{-1}). Interestingly, the misincorporation of dGTP opposite a template base thymine (0.2 s^{-1}) was more rapid than all other misincorporations, leading to the lowest fidelity (3.2×10^{-2}) among all mismatched base pairs. Additionally, tPolλ was found to possess weak strand-displacement activity during polymerization. These biochemical properties suggest that Polλ likely fills short-patched DNA gaps in base excision repair pathways and participates in mammalian nonhomologous end-joining pathways to repair double-stranded DNA breaks.

The base excision repair (BER)[1] pathway is one of the major mechanisms that removes damaged base residues in DNA (*1*). This mechanism involves the excision of modified DNA bases by DNA glycosylases, leaving noncoding apurinic/apyrimidinic (AP) sites in DNA. These lesions are further processed and repaired by 5′-acting AP endonucleases, 5′-deoxyribose-5-phosphate lyases (dRPases), DNA polymerases, and DNA ligases (*2*−*5*). In mammalian systems, the role of DNA polymerase β (Polβ) in BER has been well established (*3*). Polβ has two independent domains, an N-terminal dRPase domain (8 kDa) and a C-terminal polymerase domain (31 kDa) (Figure 1A) (*6*, *7*). The dRPase activity removes the 5′-deoxyribose phosphate moiety (*6*, *8*) while the polymerase domain, which has the general right-hand fold common to all replicative DNA polymerases defined by subdomains named fingers, palm, and thumb (*9*), catalyzes gap-filling synthesis in BER (*6*).

The recently discovered DNA polymerase λ (Polλ) and Polβ are members of the X-family DNA polymerases and share 33% sequence identity (*10*−*13*). Biochemical analysis has demonstrated that Polλ possesses intrinsic dRPase (*14*) and template-dependent DNA polymerase activities but lacks 3′→5′ exonuclease activity (Figure 1A) (*10*−*12*). The processivity of Polλ is low with normal template/primer DNA but is relatively high in short gaps having a 5′-phosphate group (*13*). Sequence alignment and three-dimensional structural modeling predict that the Polλ core contains the four conserved subdomains present in Polβ (*11*). The NMR structure of the dRPase domain solved recently displays a high degree of similarity with the corresponding domain in Polβ (*15*). Unlike Polβ, the N-terminal 132 amino acid residues of Polλ form a nuclear localization signal motif and a BRCT domain (Figure 1A). BRCT domains are known to mediate protein/protein and protein/DNA interactions in DNA repair mechanisms or cell cycle check point regulation upon DNA damage (*16*). A proline-rich region (residues 133−244) links the BRCT domain to the dRPase domain.

† This work was supported in part by American Chemical Society Petroleum Research Fund Grant PRF38364-G4, by American Cancer Society Grant IRG-98-278-03, and by the TriLink Biotechnologies Research Funding Program to Z.S. K.A.F. was supported by the National Institutes of Health Chemistry and Biology Interface Program at The Ohio State University (Grant T32 GM08512-08).

* To whom correspondence should be addressed. Telephone: 614-688-3706. Fax: 614-292-6773. E-mail: suo.3@osu.edu.

‡ These authors contributed equally to this work.

§ Department of Biochemistry.

|| Ohio State Biochemistry Program.

⊥ Ohio State Biophysics Program.

Molecular, Cellular, and Developmental Biology Program.

△ Comprehensive Cancer Center.

[1] Abbreviations: AP, apyrimidinic/apurinic site; BER, base excision repair; BRCT, breast cancer susceptibility gene 1 C terminus; dRPase, 5′-deoxyribose-5-phosphate lyase; DSB, double-strand break; NHEJ, nonhomologous end joining; PCNA, proliferating cell nuclear antigen; Polβ, DNA polymerase β; Polλ, DNA polymerase λ; tPolλ, truncated DNA polymerase λ.

10.1021/bi049975c CCC: $27.50
Published on Web 04/30/2004

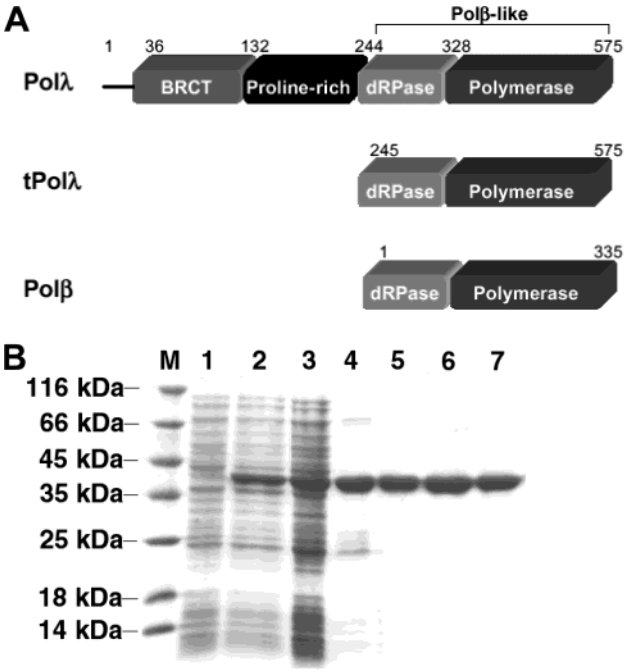

FIGURE 1: Purification of the N-terminal truncated human DNA polymerase λ. (A) Schematic representations of the full-length and truncated DNA polymerase λ as well as human DNA polymerase β. Each domain, with amino acid residue numbers indicated above, is shown as a rectangle. (B) SDS−PAGE analysis and subsequent Coomassie Blue staining of proteins at each step of the purification. Lanes: M, protein marker; 1, crude extracts of noninduced cells; 2, crude extracts of IPTG-induced cells; 3, cleared lysate; 4, eluate from the Ni affinity column; 5, eluate from the MonoS cation-exchange column; 6, eluate from the ssDNA−cellulose column; 7, loading elute from the DEAE-Sepharose column.

Truncated human Polλ (tPolλ) lacking the N-terminal 244 residues (Figure 1A) has 2.9- and 17.7-fold higher DNA polymerization activities than the full-length protein in the presence of Mg^{2+} and Mn^{2+}, respectively (*17*). Analysis of deletion mutants suggests that the proline-rich domain functionally suppresses the polymerase activity (*17*). In the presence of Mn^{2+}, both full-length Polλ and tPolλ display terminal deoxyribonucleotidyl transferase activity with sequence preference to pyrimidine nucleotides (*18*). Moreover, Polλ is shown to bypass an abasic site (*19*, *20*).

The biological function of Polλ is not clear yet although Pol$\lambda^{-/-}$ mice display hydrocephalus, situs inversus, chronic sinusitis, and male infertility (*21*). The gene encoding Polλ is mapped to mouse chromosome 19 and shown to be expressed at high level in the developing mouse testis, suggesting a possible function of Polλ in DNA repair synthesis associated with meiosis (*11*). It has been reported that proliferating cell nuclear antigen (PCNA) interacts with Polλ, increasing the processivity of Polλ in DNA synthesis without affecting either the rate of nucleotide incorporation or discrimination efficiency (*20*). These results suggest that Polλ may be involved in the PCNA-dependent "long-patch" BER pathway (*19*). In addition to the potential role in BER, human DNA Polλ is recently shown to generate single base deletions at average rates substantially higher than its base substitution rates (*22*). The high deletion frequency may rule out a significant role for Polλ in translesion synthesis and in somatic hypermutation but may suggest that Polλ is involved in repair of double-stranded breaks (DSBs) through nonhomologous end-joining (NHEJ) pathways. This hypothesis is supported by the results from immunodepletion studies suggesting that Polλ, rather than other X-family polymerases, is primarily responsible for the gap filling associated with NHEJ in human nuclear extracts (*23*).

The fidelity of Polλ has been estimated to be $(1.3-9.0) \times 10^{-4}$ by an M13mp2 forward mutation assay (*13*, *19*, *22*) and an M13mp2 reversion system (*13*, *19*, *22*). However, these mutation assays cannot provide quantitative kinetic constants to establish the mechanism of fidelity and the structure−fidelity relationship (*24*). In this study, we use pre-steady-state kinetic methods to measure the fidelity ($10^{-2}-10^{-4}$) of tPolλ on the basis of all 16 possible nucleotide incorporations into single-nucleotide gapped DNA substrates. The reason we used tPolλ rather than the full-length protein was due to strong dNTP substrate inhibition on nucleotide incorporation by the full-length Polλ (*13*, *17*). Our results showed that tPolλ catalyzed the T·dGMP misincorporation with substantially higher rates than all other mismatches. We also established a minimal mechanism of DNA polymerization catalyzed by tPolλ. The potential *in vivo* role of Polλ was discussed.

MATERIALS AND METHODS

Materials. These chemicals were purchased from the following companies: [γ-^{32}P]ATP, Perkin-Elmer Life Sciences (Boston, MA); Biospin columns, Bio-Rad Laboratories (Hercules, CA); calf intestine alkaline phosphatase, Fermentas (Hanover, MD); dNTPs, Gibco-BRL (Rockville, MD); *Pfu* turbo, Stratagene (La Jolla, CA); T4 polynucleotide kinase, USB (Cleveland, OH).

Cloning and Purification of N-Terminal Truncated Polymerase λ. The human gene encoding tPolλ (residues 245−575) was PCR amplified from a plasmid, pET28b-Polλ, encoding the full-length Polλ (K. A. Fiala and Z. Suo, unpublished results) using the following primers: β-like.for, 5′-GCGTCCATATGTCAAGCCAGAAGGCGACCAATC-3′, and β-like.rev, 5′-GCAATTCTCGAGTCACCAGTC-CCGCTCAG-3′. The resulting PCR product was cloned into the *Nde*I/*Xho*I sites of pET24b to construct pET24b-tPolλ. The constructed plasmid pET24b-tPolλ was transformed into *Escherichia coli* strain BL21(DE3)pLysS (Stratagene) to express tPolλ fused to a C-terminal His_6 tag. Transformed *E. coli* cells were grown at 37 °C in the presence of 40 μg/mL kanamycin and 50 μg/mL chloramphenicol until OD_{600} reached 0.5. Then the cultures were induced with 0.4 mM IPTG and incubated at 22 °C for 7 h. Cells were harvested (4000 rpm, 15 min) and resuspended in buffer A (10 mM potassium phosphate, pH 7.0, 0.5 M NaCl, 10 mM $MgCl_2$, 10% glycerol, 0.1% β-mercaptoethanol, 5 mM imidazole). After the addition of 2 mM PMSF, resuspended cells were lysed by passing through a French press cell at 16000 psi three times, and the resulting lysate was cleared by spinning in an ultracentrifuge (40000 rpm, 40 min). After overnight incubation of cleared lysate with nickel-NTA resin (Qiagen), the tPolλ in the supernatant was purified through a linear gradient of 20−500 mM imidazole in buffer B (10 mM potassium phosphate, pH 7.0, 0.35 M NaCl, 2.5 mM $MgOAc_2$, 10% glycerol, 0.1% β-mercaptoethanol). tPolλ-containing fractions were pooled and dialyzed against buffer C (50 mM Tris-HCl, pH 7.0, 25 mM NaCl, 10% glycerol, 2 mM EDTA, 0.1% β-mercaptoethanol) at 4 °C. The dialyzed

Table 1: DNA 21-19/41-mer Substrates[a]

D-1	5′-CGCAGCCGTCCAACCAACTCA CGTCGATCCAATGCCGTCC-3′
	3′-GCGTCGGCAGGTTGGTTGAGTAGCAGCTAGGTTACGGCAGG-5′
D-6	5′-CGCAGCCGTCCAACCAACTCA CGTCGATCCAATGCCGTCC-3′
	3′-GCGTCGGCAGGTTGGTTGAGTGGCAGCTAGGTTACGGCAGG-5′
D-7	5′-CGCAGCCGTCCAACCAACTCA CGTCGATCCAATGCCGTCC-3′
	3′-GCGTCGGCAGGTTGGTTGAGTTGCAGCTAGGTTACGGCAGG-5′
D-8	5′-CGCAGCCGTCCAACCAACTCA CGTCGATCCAATGCCGTCC-3′
	3′-GCGTCGGCAGGTTGGTTGAGTCGCAGCTAGGTTACGGCAGG-5′
D-12	5′-CGCAGCCGTCCAACCAACTCA TGTCGATCCAATGCCGTCC-3′
	3′-GCGTCGGCAGGTTGGTTGAGTCACAGCTAGGTTACGGCAGG-5′

[a] The downstream 19-mer primer was 5′-phosphorylated. The top strand was composed of two oligonucleotides (21-mer and 19-mer) with a single-nucleotide gap between them.

protein solution was passed through a 10 mL DEAE-Sepharose column (Amersham Pharmacia Biotech). The loading elute was applied to a MonoS 10/10 column (Amersham Pharmacia Biotech) and eluted using a gradient of 50−700 mM NaCl in buffer D (25 mM HEPES, pH 7.5, 50 mM NaCl, 10% glycerol, 1 mM EDTA, 0.1% β-mercaptoethanol). The fractions containing tPolλ were pooled and dialyzed against buffer D. The dialyzed protein solution was loaded into a prepacked ssDNA−cellulose column (Sigma). After washing, tPolλ was then eluted with a 50−1000 mM NaCl gradient in buffer C. The fractions containing tPolλ were pooled and dialyzed against buffer D. The dialyzed tPolλ was passed through a 10 mL DEAE-Sepharose column. The loading elute was dialyzed against buffer D and concentrated using a Centriprep YM-30 (Millipore). The concentrated protein was ultimately dialyzed against buffer E (25 mM HEPES, pH 7.5, 50 mM NaCl, 1 mM EDTA, 1 mM DTT, 50% glycerol). tPolλ was purified to >95% purity on the basis of SDS−PAGE analysis (Figure 1B). The concentration of the purified tPolλ was measured spectrophotometrically at 280 nm using the calculated extinction coefficient of 39367 M^{-1} cm^{-1}.

Synthetic Oligonucleotides. The DNA substrates listed in Table 1 were purchased from either Integrated DNA Technologies or TriLink Biotechnologies and purified by denaturing polyacrylamide gel electrophoresis (18% acrylamide, 8 M urea), and the concentration was determined by UV absorbance at 260 nm with the following extinction coefficients (M^{-1} cm^{-1}): primer 19-mer, $\epsilon = 171000$; primer 21-mer, $\epsilon = 194100$; D-1 template 41-mer, $\epsilon = 396700$; D-6 template 41-mer, $\epsilon = 394200$; D-7 template 41-mer, $\epsilon = 392200$; D-8 template 41-mer, $\epsilon = 389500$; D-12 template 41-mer, $\epsilon = 392400$. The primer strand 21-mer was 5′-^{32}P labeled by incubation with T4 polynucleotide kinase and [γ-^{32}P]ATP for 1 h at 37 °C. The unreacted [γ-^{32}P]ATP was subsequently removed by centrifugation via a Bio-Spin-6 column (Bio-Rad). The 5′-^{32}P-labeled primer 21-mer was then annealed with the corresponding nonradiolabeled downstream primer 19-mer and template 41-mer at a molar ratio of 1.0:1.15:1.25, respectively, to form the 21-19/41-mer single-nucleotide gapped substrate (the top strand was composed of two oligonucleotides with a single-nucleotide gap). Mixtures to be annealed were denatured at 95 °C for 8 min and then cooled slowly to room temperature over several hours.

Optimized Reaction Buffer L. All experiments using tPolλ, if not specified, were performed in buffer L containing 50 mM Tris-HCl (pH 8.4 at 37 °C), 5 mM $MgCl_2$, 100 mM NaCl, 0.1 mM EDTA, 5 mM DTT, 10% glycerol, and 0.1 mg/mL BSA. All reactions were carried out at 37 °C.

Rapid Quench Experiments. Experiments were carried out in a rapid chemical quench-flow apparatus manufactured by KinTek (Clarence, PA). The experiments were carried out by allowing enzyme and DNA to preincubate in buffer L. An aliquot of this solution (15 μL) was rapidly mixed with an equal volume of solution of the incoming nucleotide in buffer L. The reactions were quenched with 90 μL of 0.37 M EDTA (final concentration) after time intervals ranging from milliseconds to several minutes. All concentrations reported in this paper refer to concentrations during the reaction following rapid mixing.

Measurement of the Equilibrium Dissociation Constant of the Next Incoming Nucleotide. A preincubated solution of tPolλ and a gapped DNA substrate at fixed concentrations was mixed at varying concentrations of Mg^{2+}-dNTP (0.25−120 μM) in buffer L at 37 °C to start the reaction. The reactions at each concentration of Mg^{2+}-dNTP were terminated with 0.37 M EDTA at varying times from milliseconds to minutes. The reaction products were analyzed by sequencing gel analysis. The time course of product formation was fit to a single exponential equation (see Data Analysis) for each concentration of Mg^{2+}-dNTP to give the observed rate constant of nucleotide incorporation. Then, the observed rates extracted from these time courses of product formation were plotted against the concentrations of Mg^{2+}-dNTP, and these data were fit via hyperbolic regression (see Data Analysis) to give the equilibrium dissociation constant of dNTP, K_d, and the maximum rate constant for incorporation of dNTP, k_p.

Measurement of the Dissociation Rate Constant of the Next Incoming Nucleotide. tPolλ (60 nM), unlabeled D-8 (300 nM), [α-^{32}P]dGTP (20 μM), and EDTA (0.5 mM) were preincubated in a buffer which was identical to buffer L except it lacked Mg^{2+} to form the tPolλ·DNA·[α-^{32}P]dGTP ternary complex. This preincubated solution was reacted with a solution containing a large molar excess of unlabeled dGTP (2 mM) and Mg^{2+} (5.5 mM) for various time intervals prior to being quenched by 0.37 M EDTA. The reaction mixtures were analyzed as described below.

Measurement of the Dissociation Rate Constant of the 21-19/41-mer. A preincubated solution of tPolλ (60 nM), unlabeled D-8 (300 nM), [α-^{32}P]dGTP (20 μM), and 0.5 mM EDTA in a buffer which was identical to buffer L except it lacked Mg^{2+} was reacted with a solution containing Mg^{2+} (5.5 mM) with no additional dGTP for various time intervals. The reactions were subsequently stopped by the addition of EDTA (0.37 M) and analyzed as described below.

Product Analysis. Reaction products were analyzed by sequencing gel electrophoresis (17% acrylamide, 8 M urea, 1× TBE buffer) and quantitated with a PhosphorImager 445 SI (Molecular Dynamics).

Data Analysis. Data were fit by nonlinear regression using the program KaleidaGraph (Synergy Software). The single turnover experimental data were fit to eq 1 (single exponential), where A represents the reaction amplitude, which

$$[\text{product}] = A[1 - \exp(-k_{obs}t)] \quad (1)$$

is equal to the initial concentration of the enzyme and DNA binary complex, and k_{obs} is the observed single turnover rate constant. Data from measurement of K_d of dNTP were fit to eq 2 (hyperbola), where k_p is the maximum rate constant of

$$k_{obs} = k_p[\text{dNTP}]/\{[\text{dNTP}] + K_d\} \quad (2)$$

dNTP incorporation. The substrate specificity and polymerase fidelity were calculated as (k_p/K_d) and $(k_p/K_d)_{incorrect}/[(k_p/K_d)_{correct} + (k_p/K_d)_{incorrect}]$, respectively. Data from the measurement of the nucleotide dissociation rate constant (k_{off}) were fit to eq 3. Data from the [α-^{32}P]dNTP incorporation

$$[\text{product-3}'\text{-}^{32}\text{P}] = [k_p/(k_p + k_{off})][\text{E}\cdot\text{DNA}\cdot\text{dNTP-}^{32}\text{P}][1 - \exp(-k_p t)] \quad (3)$$

experiment were fit to eq 4 (*25*, *26*), where k_1 is the DNA

$$[\text{product}] = \{[k_{obs}k_1 t/(k_{obs} + k_1)] + [k_{obs}/(k_{obs} + k_1)]^2\{1 - \exp[-(k_{obs} + k_1)t]\}\}[\text{E}_0] \quad (4)$$

dissociation rate constant, k_{obs} is the observed nucleotide incorporation rate constant, and $[E_0]$ is the initial enzyme active concentration.

RESULTS

To kinetically define the fidelity and substrate specificity of a polymerase, we need to measure the dependence of nucleotide incorporation rates on nucleotide concentration. However, nucleotide incorporation by the full-length Polλ is inhibited when the nucleotide concentration is over 1 μM (*13*, *17*). In the kinetic studies of the full-length human Polλ purified in our laboratory, we confirmed the observation of substrate inhibition (W. Abdel-Gawad and Z. Suo, unpublished results). Since the proline-rich domain is determined to be the suppressor on the basis of protein truncation studies (*17*), we decided to prepare tPolλ (residues 245−575, Figure 1A) and measure the kinetic parameters and fidelity of this fragment, which does not contain the BRCT and proline-rich domains and should not exhibit substrate inhibition. Our kinetic experiments demonstrated that tPolλ was active and no substrate inhibition was observed for this truncated enzyme (see below). tPolλ and Polβ share 33% sequence identity including critical residues involved in nucleotide and DNA binding and catalysis (*10*−*13*). Thus, tPolλ allowed us to estimate the intrinsic fidelity of the full-length Polλ.

Protein Purification. The C-terminal hexahistidine-tagged tPolλ (38.2 kDa) was overexpressed in *E. coli* BL21(DE3) and purified to homogeneity (Figure 1B) through Ni affinity, MonoS cation-exchange, single-stranded DNA−cellulose affinity, and DEAE-Sepharose ion-exchange columns (see Materials and Methods). The yield was approximately 10 mg/L of initial *E. coli* culture. The N-terminal eight amino acid residues were confirmed by protein sequencing while the C-terminal hexahistidine tag was detected by Western blot analysis using anti-hexahistidine-tagged antibody (data not shown).

Optimization of Reaction Conditions. Our first objective was to optimize the reaction conditions for nucleotide incorporation by tPolλ. To optimize these conditions, we held all components constant while independently varying $MgCl_2$ concentration, NaCl concentration, and pH. In these assays, a solution of 30 nM 5′-^{32}P-labeled D-1 (Table 1) was preincubated with a 3-fold excess of tPolλ and subsequently mixed with 100 μM dTTP at 37 °C using a rapid chemical quench apparatus. The reactions were quenched by the addition of 0.37 M EDTA at various time intervals. The DNA product 22-mer and unreacted substrate 21-mer were then separated via gel electrophoresis and subsequently quantitated using a phosphorimager. The data were fit to eq 1 (see Materials and Methods). The single turnover rate constant (k_{obs}) varied with the $MgCl_2$ concentration, NaCl concentration, and the buffer pH in the three aforementioned assays. Notably, in determining the optimal $MgCl_2$ concentration, we observed a significant decrease in reaction amplitude as we incrementally increased the concentration of $MgCl_2$ (Figure 2A). The amplitude decrease was likely due to high ionic strength caused by high $MgCl_2$ concentration which may inhibit polymerization either by disrupting the interactions between tPolλ and its substrates (DNA and nucleotide) or by forming a nonproductive ternary complex of tPolλ·DNA·dNTP (*27*−*29*). Interestingly, the observed single turnover rate constants increased with increasing $MgCl_2$ concentration (Figure 2A). The reason for this result is not clearly understood at present. Interestingly, the effect of $MgCl_2$ concentration on k_{obs} has also been found in single-nucleotide incorporation catalyzed by rat DNA polymerase β (*30*) and *Sulfolobus solfataricus* P2 DNA polymerase IV (*31*). Since the increase in $MgCl_2$ concentration was concomitant with both an increase in the single turnover rate constant and a decrease in reaction amplitude, we decided to compromise at an optimal $MgCl_2$ concentration of 5 mM $MgCl_2$, which was the highest $MgCl_2$ concentration that still retained full single turnover reaction amplitude (Figure 2A).

With the exception of the time courses carried out at the nonphysiological pH conditions of 6.0 and 10, we did not observe any other aberrations in regard to reaction amplitude in the optimization process for either pH (Figure 2C) or NaCl concentration (Figure 2B). The low reaction amplitudes observed at pH 6 and 10 indicated that the ternary complex of tPolλ·DNA·dNTP became partially nonproductive due to the acidic or basic reaction conditions. The results obtained from the optimization experiments for tPolλ polymerization were 5 mM $MgCl_2$ (Figure 2A), 100 mM NaCl (Figure 2B), and pH 8.4 (Figure 2C). Thus, the optimized reaction buffer contains 50 mM Tris-HCl, pH 8.4, 5 mM $MgCl_2$, 100 mM NaCl, 0.1 mM EDTA, 5 mM DTT, 10% glycerol, and 0.1 mg/mL BSA (buffer L). In addition, similar single turnover rate constants and full reaction amplitudes were observed with a 9-fold excess of enzyme over DNA (data not shown). This indicated that the 3-fold excess of enzyme over DNA was enough to ensure that almost all of the DNA molecules were bound by tPolλ, which satisfied the single turnover conditions.

Rapid Equilibrium of Nucleotide Binding. The kinetic mechanism of single-nucleotide incorporation into a synthetic primer/template substrate catalyzed by many DNA polymerases has been studied by employing pre-steady-state kinetic methods (*32*−*39*). The minimal mechanism shared by all DNA polymerases studied to this point, including DNA polymerase β (*35*), is shown in Scheme 1. In this scheme, the binary complex of enzyme and DNA ($E\cdot DNA_n$) binds an incoming nucleotide (dNTP) to form a ground-state ternary complex $E\cdot DNA_n\cdot dNTP$. This ternary complex

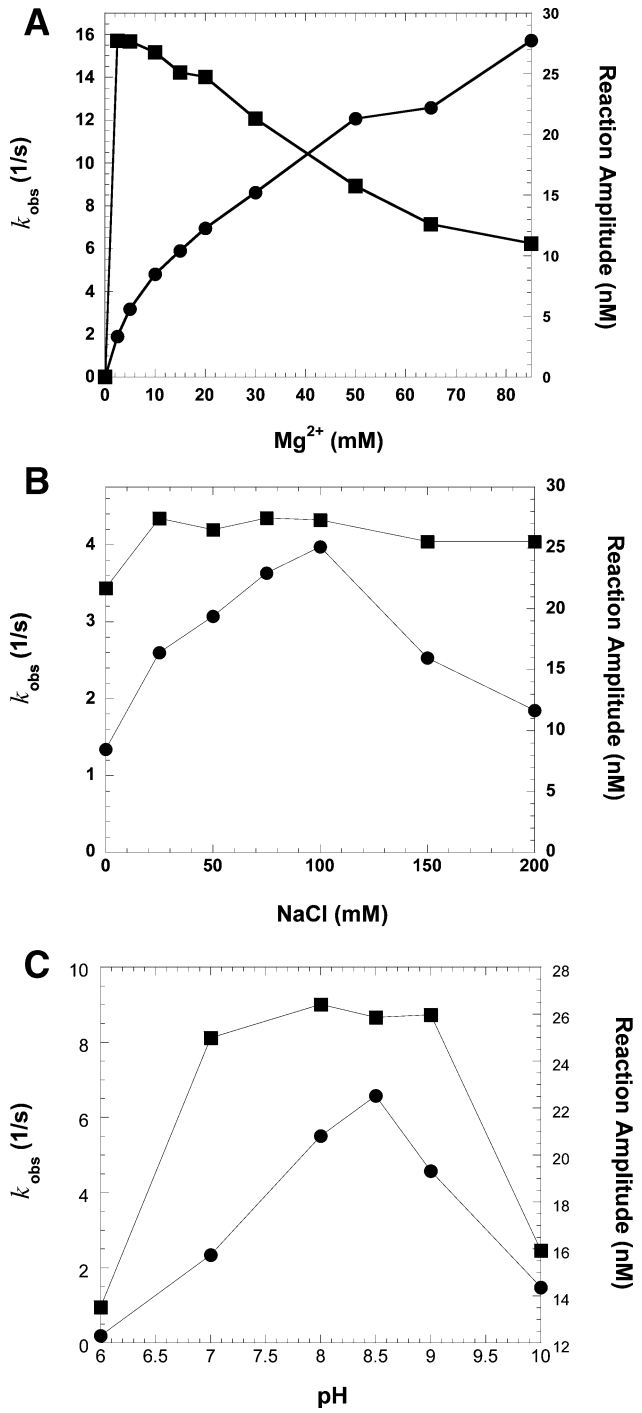

FIGURE 2: Optimization of the reaction conditions for tPolλ. Effects of Mg^{2+} concentration, NaCl concentration, and buffer pH on the activity of tPolλ at 37 °C. A preincubated solution of 5′-^{32}P-labeled D-1 (30 nM) and a 3-fold excess of tPolλ (120 nM) was mixed with correct incoming nucleotide (100 μM dTTP) for various reaction times under single turnover conditions. Concentrations of all components were held constant while (A) Mg^{2+} concentration, (B) NaCl concentration, or (C) buffer pH was varied independently. Reaction rate constants (k_{obs}, s^{-1}) (●) and reaction amplitudes (nM) (■) were plotted simultaneously. The activity in (C) was assayed in 25 mM MES-NaOH buffer between pH 6.0 and 7.0, 25 mM Tris-HCl buffer for pH 8.0 and 8.5, and 25 mM glycine-NaOH buffer for pH 9.0 and 10.0.

undergoes both a protein conformational change and chemical reaction to form the product-containing ternary complex, E·DNA$_{n+1}$·PP$_i$. Notably, these two steps are simplified into one step as shown in Scheme 1. During this step, the DNA primer is elongated by one nucleotide and pyrophosphate (PP$_i$) is formed. For subsequent turnovers to occur in single-nucleotide incorporation, the enzyme has to dissociate from the product ternary complex. Our kinetic analysis described below suggested that Scheme 1 was the kinetic pathway for DNA polymerization catalyzed by tPolλ.

To evaluate whether the binding of an incoming nucleotide was at rapid equilibrium (k_{on}, $k_{off} \gg k_p$), we carried out an experiment to assess the relative rate constants of dNTP dissociation (k_{off}) and nucleotide polymerization (k_p) (Scheme 1). Here, we mixed a preincubated solution of tPolλ, 5-fold unlabeled D-8, and [α-^{32}P]dGTP (20 μM) in the optimized buffer lacking Mg^{2+} and containing EDTA (0.5 mM) with a solution containing a large molar excess of unlabeled dGTP (2 mM) and Mg^{2+} for various reaction times followed by quenching with EDTA. Although tPolλ was purified and stored in the absence of divalent metal ions, we used additional 0.5 mM EDTA present in the preincubated enzyme solution to chelate any contaminant divalent cations carried over from the protein purification. This concentration of EDTA was shown to be sufficient to prevent any product formation in this preincubated solution (data not shown). If the dissociation of dNTP from the E·DNA·dNTP ternary complex was much faster than the polymerization, we would expect to see very little 3′-α-^{32}P-labeled product formation due to the unfavorable kinetic partitioning, and large molar excess of unlabeled dGTP that once bound to the E·DNA binary complex would remove the ternary complex from observation. This assay resulted in a time course showing an insignificant amount of radiolabeled product (approximately 1 nM at the longest reaction time in Figure 3 inset). Additionally, each product concentration in this time course was corrected for the contribution to product formation from the incorporation of dissociated [α-^{32}P]dGTP as measured in a control experiment. In this control experiment, we preincubated a solution of tPolλ (60 nM), unlabeled D-8 (300 nM), and unlabeled dGTP (20 μM) in the optimized buffer lacking Mg^{2+} and containing 0.5 mM EDTA and then mixed this solution with another solution containing a large molar excess of unlabeled dGTP (1.98 mM), 20 μM [α-^{32}P]dGTP, and Mg^{2+} (5.5 mM) for various reaction times.

The time course (●) shown in Figure 3 was fit to eq 3 (see Materials and Methods) to obtain the nucleotide dissociation rate constant from the E·DNA·[^{32}P]dNTP complex. The measured k_{off} and k_p are 300 ± 100 s^{-1} and 6 ± 2 s^{-1}, respectively. Thus, the nucleotide dissociation rate constant was indeed faster than the polymerization rate constant. Moreover, the association rate constant of the binding of dGTP to the tPolλ·D-8 binary complex, $k_{on} = k_{off}/K_d = 1.55 \times 10^8$ M^{-1} s^{-1}, was calculated from the values of k_{off} (300 s^{-1}) and K_d (1.93 μM), which was measured below. This suggested that the binding of a nucleotide to the binary complex tPolλ·DNA was rapid and under diffusion control. Therefore, the binding of a nucleotide to form the ground-state ternary complex tPolλ·DNA·dNTP was at rapid equilibrium. Such a fast equilibrium has been observed with the Klenow fragment of *E. coli* DNA polymerase I (*40*), T7 DNA polymerase (*34*), and *S. solfataricus* P2 DNA polymerase IV (*32*). This rapid equilibrium of nucleotide binding, which was much faster than the polymerization, allows us to measure the ground-state binding affinity of an incoming nucleotide.

Scheme 1

$$E{\bullet}DNA_n + dNTP \underset{k_{off}}{\overset{k_{on}}{\rightleftharpoons}} E{\bullet}DNA_n{\bullet}dNTP \overset{k_p}{\rightleftharpoons} E{\bullet}DNA_{n+1}{\bullet}PPi \overset{k_1}{\rightleftharpoons} E + DNA_{n+1} + PPi$$

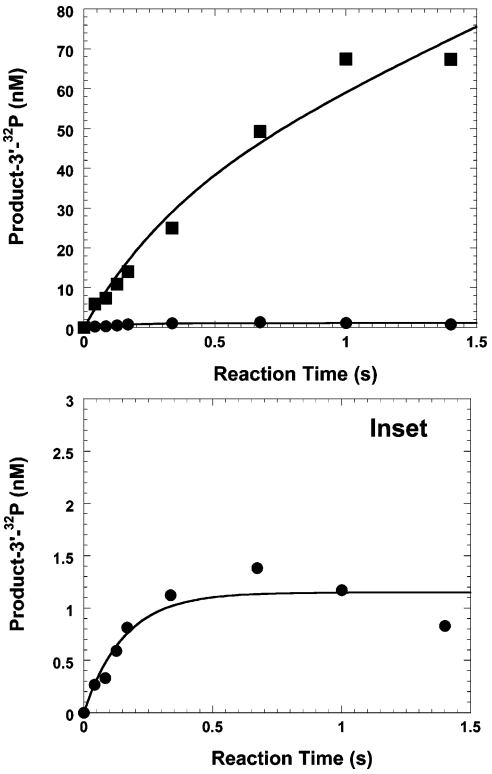

FIGURE 3: Measurements of dNTP (k_{off}) and DNA (k_1) dissociation rate constants and the nucleotide polymerization rate constant (k_p). In the second time course, a preincubated solution of tPolλ (60 nM), unlabeled D-8 (300 nM), [α-^{32}P]dGTP (20 μM), and 0.5 mM EDTA in the absence of Mg^{2+} was reacted with a solution containing a large molar excess of unlabeled dGTP (2 mM) and Mg^{2+} (5.5 mM) for various reaction times (●) (see figure inset). The product concentrations in this time course were corrected for the contribution to product formation from the incorporation of dissociated [α-^{32}P]dGTP (see text). The data (●) were fit to eq 3 (see Materials and Methods) to obtain the nucleotide dissociation rate constant (k_{off}) from the E·DNA·[^{32}P]dNTP complex. The measured k_{off} and k_p are 300 ± 100 and 6 ± 2 s^{-1}, respectively. In the second time course, a preincubated solution of tPolλ (60 nM), unlabeled D-8 (300 nM), [α-^{32}P]dGTP (20 μM), and 0.5 mM EDTA in the absence of Mg^{2+} was reacted with a solution containing Mg^{2+} (5.5 mM) with no additional unlabeled dGTP for various reaction times (■). The data were fit to eq 4 (see Materials and Methods) to obtain a k_p of 2.1 ± 0.3 s^{-1} and a fast DNA dissociation rate constant (k_1) of 0.8 ± 0.3 s^{-1}.

Measurement of the DNA Dissociation Rate Constant. To ensure that the above nucleotide incorporation rate constant was not affected by preincubating the E·DNA·dNTP ternary complex in the absence of Mg^{2+}, we performed another control experiment. In this experiment, a preincubated solution of tPolλ (60 nM), unlabeled D-8 (300 nM), [α-^{32}P]dGTP (20 μM), and EDTA (0.5 mM) in the optimized buffer lacking Mg^{2+} was reacted with a solution containing Mg^{2+} and no additional unlabeled trap dGTP for various reaction times. This experiment yielded a time course of product formation (■) (Figure 3) that was very similar to that obtained when a preincubated tPolλ·DNA binary complex in the presence of Mg^{2+} reacted with dNTP·Mg^{2+} (data not shown). This suggested that the binding of nucleotide was rapid and the nucleotide incorporation was not affected by preincubating the E·DNA·dNTP ternary complex in the absence of Mg^{2+}. The data (■) were fit to eq 4 (see Materials and Methods) to obtain a k_{obs} of 2.1 ± 0.3 s^{-1} and a DNA dissociation rate constant (k_1 in Scheme 1) of 0.8 ± 0.3 s^{-1}. The smaller observed polymerization rate constant k_{obs} in comparison to the k_p values obtained above and below was due to the unsaturated dNTP concentration used in this experiment. The reason the data (■) were not fit into a burst equation was because the k_{obs} value was not significantly larger than k_1 (*25*, *26*). The comparable k_{obs} and k_1 values prevent the appearance of an obvious burst phase in the time course (■).

Substrate Specificity of the Correct Nucleotide. The ground-state binding affinity of dTTP (K_d) to the E·DNA binary complex (Scheme 1) was measured through the dTTP concentration dependence of the single turnover rate constant (k_{obs}). The single turnover method was employed because the above measured DNA dissociation rate constant (k_1) was high and the burst phase was not obvious in Figure 3. The experiments were performed with enzyme in molar excess over DNA substrate to allow the direct observation of nucleotide incorporation in a single pass of the reactants through the enzymatic pathway without complications resulting from the steady-state formation of products (*26*). A preincubated solution of 5′-radiolabeled D-1 and 4-fold tPolλ was reacted with increasing concentrations of dTTP in buffer L. The DNA product 22-mer and unextended substrate 21-mer at different time intervals were separated and quantitated as described in detail in Materials and Methods. The product concentration was plotted against reaction time intervals. The data were subsequently fit to a single exponential, eq 1 (see Materials and Methods), to yield a single turnover rate constant at each concentration of dTTP (Figure 4A). The single turnover rates were then plotted against dTTP concentrations (Figure 4B). The data were subsequently fit to a hyperbolic equation, eq 2 (see Materials and Methods), to yield a k_p of 6.0 ± 0.2 s^{-1} for the maximum dTTP incorporation rate constant and a K_d of 2.4 ± 0.4 μM for dTTP binding. Additionally, the value of the substrate specificity (k_p/K_d) was calculated to be 2.5 μM^{-1} s^{-1} (Table 2).

Similar analyses implementing single turnover conditions were used to determine the kinetic parameters (k_p, K_d, and k_p/K_d) for the incorporations of the other three correct nucleotides, dCTP into D-6, dATP into D-7, and dGTP into D-8 (data not shown), and the parameters are listed in Table 2. The ground-state binding affinity and, moreover, the substrate specificity of all four correct nucleotide incorporations under single turnover conditions were similar. The binding affinity of correct nucleotides to the tPolλ·DNA binary complex is similar to that observed in Polβ with a single-nucleotide gapped DNA (*41*).

Substrate Specificity of the Incorrect Nucleotide. Pre-steady-state kinetic analysis of incorrect dGTP incorporation into D-1 was assayed by implementing similar single turnover kinetic methods as described above. tPolλ was

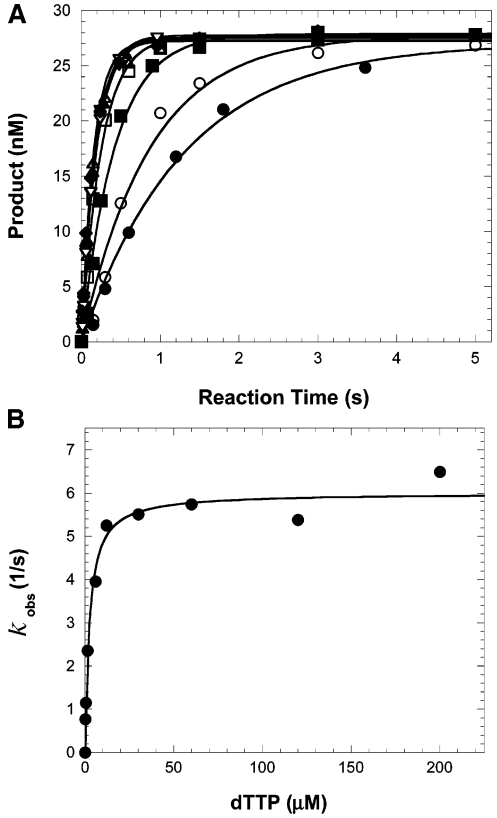

FIGURE 4: Concentration dependence on the pre-steady-state rate constant of correct nucleotide incorporation. (A) A preincubated solution of tPolλ (120 nM) and 5′-^{32}P-labeled D-1 (30 nM) was mixed with increasing concentrations of Mg^{2+}-dTTP (0.25 μM, ●; 0.5 μM, ○; 1.5 μM, ■; 6 μM, □; 12 μM, △; 30 μM, ▲; 60 μM, ▼; 120 μM, ▽; 200 μM, ◆) for various time intervals. The solid lines are the best fits to the single exponential equation (eq 1). (B) The single exponential rates obtained from the above data fitting were plotted as a function of dTTP concentration. The data (●) were then fit to the hyperbolic equation (eq 2), yielding a k_p of 6.0 ± 0.2 s^{-1} and a K_d of 2.4 ± 0.4 μM.

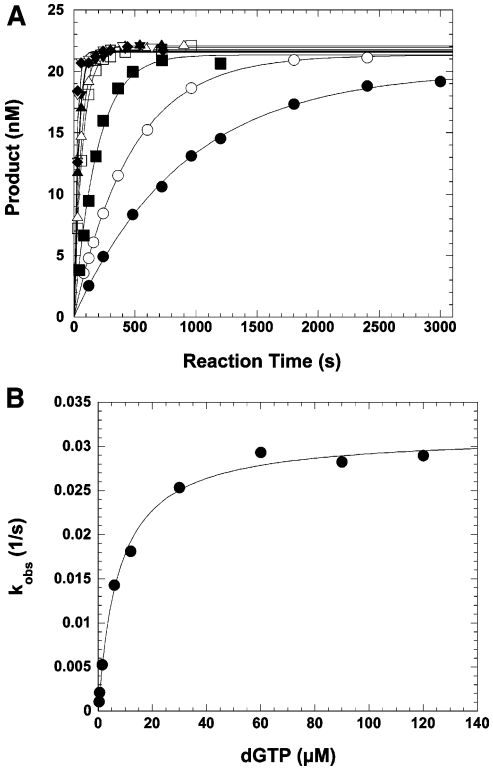

FIGURE 5: Concentration dependence on the pre-steady-state rate constant of incorrect dGTP incorporation. (A) A preincubated solution of tPolλ (120 nM) and 5′-^{32}P-labeled D-1 (30 nM) was mixed with increasing concentrations of Mg^{2+}-dGTP (0.25 μM, ●; 0.5 μM, ○; 1.5 μM, ■; 6 μM, □; 12 μM, △; 30 μM, ▲; 60 μM, ▼; 100 μM, ▽; 120 μM, ◆) for various time intervals. The solid lines are the best fits to the single exponential equation. (B) The single exponential rates obtained from the above data fitting were plotted as a function of dGTP concentration. The data (●) were then fit to the hyperbolic equation, yielding a k_p of 0.022 ± 0.001 s^{-1} and a K_d of 8.4 ± 0.7 μM.

preincubated with 5′-radiolabeled D-1 and was then reacted with increasing concentration of dGTP in buffer L. The reactions were manually quenched with EDTA and analyzed via gel electrophoresis, and the products were quantitated using a phosphorimager. The single turnover rate constant observed at each concentration of dGTP was obtained through the fit of the time course of product formation to eq 1 (Figure 5A). The observed reaction rates were then plotted against the concentrations of dGTP, and these data were fit by nonlinear regression into eq 2 (see Materials and Methods) to obtain k_p, K_d, and substrate specificity (k_p/K_d) of 0.022 ± 0.001 s^{-1}, 8.4 ± 0.7 μM, and 2.6 × 10^{-3} μM^{-1} s^{-1}, respectively (Table 2 and Figure 5B).

With DNA substrates D-1, D-6, D-7, and D-8 the kinetic parameters for each nucleotide of the remaining 11 possible incorrect single-nucleotide incorporations were determined under the same single turnover conditions (Table 2). On average, the incorrect nucleotide incorporations have only about 2-fold lower ground-state binding affinity (K_d) and 1−3 orders of magnitude slower incorporation rates when compared to the four correct nucleotide incorporations. Since the tight binding of mismatched nucleotides was surprising, we repeated the measurements of the misincorporations and obtained values similar to those listed in Table 2. In addition, we measured the kinetic parameters of dCTP incorporation into D-7 in the presence of a 9-fold, rather than 3-fold (Table 2), excess of enzyme over DNA (data not shown). The values

Table 2: Pre-Steady-State Kinetic Parameters of tPolλ

dNTP	K_d (μM)	k_p (s^{-1})	k_p/K_d ($\mu M^{-1} s^{-1}$)	fidelity[a]
		Template A (D-1)		
dATP	3.6 ± 0.5	0.0010 ± 0.0008	2.8×10^{-4}	1.1×10^{-4}
dTTP	2.4 ± 0.4	6.0 ± 0.2	2.5	1
dGTP	8.4 ± 0.7	0.022 ± 0.001	2.6×10^{-3}	1.1×10^{-3}
dCTP	5.4 ± 0.4	0.062 ± 0.003	1.1×10^{-2}	4.6×10^{-3}
		Template G (D-6)		
dATP	2.4 ± 0.7	0.0016 ± 0.0001	6.7×10^{-4}	2.5×10^{-4}
dTTP	1.8 ± 0.7	0.0115 ± 0.0007	6.3×10^{-3}	2.4×10^{-3}
dGTP	3.2 ± 0.4	0.0021 ± 0.0008	6.5×10^{-4}	2.5×10^{-4}
dCTP	1.1 ± 0.3	3.0 ± 0.2	2.7	1
		Template T (D-7)		
dATP	1.7 ± 0.2	3.87 ± 0.08	2.2	1
dTTP	1.9 ± 0.3	0.004 ± 0.001	2.1×10^{-3}	1.0×10^{-3}
dGTP	2.9 ± 1.4	0.20 ± 0.02	7.1×10^{-2}	3.2×10^{-2}
dCTP	1.9 ± 0.6	0.015 ± 0.002	7.8×10^{-3}	3.5×10^{-3}
		Template C (D-8)		
dATP	1.4 ± 0.3	0.0046 ± 0.0001	3.2×10^{-3}	1.5×10^{-3}
dTTP	4.7 ± 0.5	0.0065 ± 0.0001	1.4×10^{-3}	6.4×10^{-4}
dGTP	1.9 ± 0.4	4.1 ± 0.2	2.1	1
dCTP	1.5 ± 0.2	0.0098 ± 0.0002	6.4×10^{-3}	3.0×10^{-3}
		Template C (D-12)		
dTTP	3.4 ± 0.9	0.0110 ± 0.0005	3.2×10^{-3}	
dCTP	4.4 ± 1.4	0.0051 ± 0.0003	1.1×10^{-3}	

[a] Calculated as $(k_p/K_d)_{incorrect}/[(k_p/K_d)_{correct} + (k_p/K_d)_{incorrect}]$.

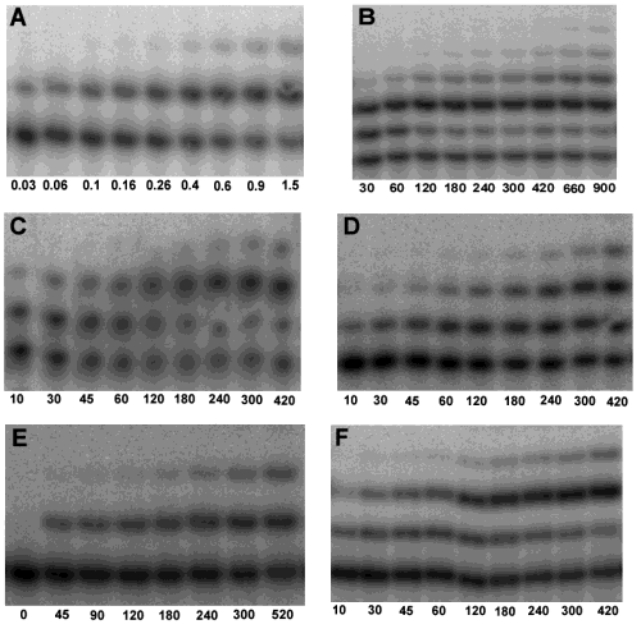

FIGURE 6: Series of gel pictures showing the progression of product formation as a function of time under conditions of 100 μM dNTP for each of the following nucleotide incorporations: (A) dCTP into D-6, (B) dCTP into D-1, (C) dCTP into D-7, (D) dCTP into D-8, (E) dCTP into D-12, and (F) dTTP into D-12. Unreacted substrate (21-mer) is shown at the bottom of each gel picture with extended products located sequentially above the corresponding unreacted substrate. Reaction time intervals (seconds) are denoted below the corresponding lane.

of k_p and K_d differed less than 5% of those listed in Table 2. This result not only confirmed the above conclusion that a 3-fold excess of enzyme over DNA was enough to satisfy the single turnover conditions but also indicated that the tighter binding of an incorrect nucleotide to the tPolλ·DNA binary complex was not due to fast DNA dissociation.

Interestingly, while dGTP binding to the E·D-7 binary complex, which forms the T·dGMP wobble base pair, was characteristic of incorrect nucleotide incorporation for tPolλ, the maximum rate constant of polymerization (k_p) was 10−100-fold faster than typical incorrect incorporations, leading to its apparent higher substrate specificity. In contrast, the kinetic parameters for the dTTP incorporation into D-6 to form the G·dTMP mismatch base pair were similar to those of other mismatches. This apparent asymmetry was observed only with these two mismatches.

The values of substrate specificity and fidelity (see Materials and Methods) for all 12 incorrect incorporations were calculated and listed in Table 2. The fidelity of tPolλ with the single-nucleotide gapped DNA is in the range of 10^{-2}−10^{-4}, and it has the lowest value for the T·dGMP wobble base pair.

Strand-Displacement Activity. For the incorporation of the correct nucleotide dCTP into D-6, we observed the formation of both 22-mer and 23-mer products (Figure 6A). The formation of the 23-mer was due to a second dCTP incorporation opposite the downstream template base G, which was initially base paired with the downstream primer 19-mer (Table 1). We also observed a small amount of 23-mer in addition to the major product 22-mer for the incorporations of mismatched nucleotides with the exception of dCTP (data not shown). These results indicated that tPolλ had a weak strand-displacement activity. This activity was not observed for the other three correct nucleotide incorporations including dTTP into D-1, dATP into D-7, and dGTP into D-8 since only 22-mer was observed in each of these three cases (data not shown). We believe the reason for these observations is due to a combination of slow rates of misincorporation on top of the downstream template G in these three cases coupled with much shorter reaction time intervals in these assays that yielded a negligible amount of product 23-mer.

Surprisingly, the misincorporation of dCTP into D-1 (Figure 6B), D-7 (Figure 6C), and D-8 (Figure 6D) yielded products ranging from 22-mer to 26-mer, and the major product was 23-mer. Interestingly, the next two downstream template bases of the three DNA substrates are G followed by C. The incorporation of a second dCTP against the template G was matched and fast while the third dCTP incorporation was mismatched opposite the template C and slow, leading to the accumulation of the 23-mer. The downstream template base G seemed to facilitate the strand-displacement activity of tPolλ in the multiple incorporations of dCTP. To prove this hypothesis, we changed the next template base G in D-8 to A (D-12 in Table 1), and the incorporation of dCTP into D-12 yielded predominantly the 22-mer and a small amount of the 23-mer (Figure 6E). Moreover, the incorporation of dTTP into D-12 showed similar pattern as dCTP into D-1, D-7, and D-8: (i) three products and (ii) the 23-mer as the major product (Figure 6F). The overall substrate specificity (k_p/K_d) was 5-fold lower for dCTP incorporation into D-12 than dCTP into D-8 while 2-fold higher for dTTP into D-12 than dTTP into D-8 (Table 2). These results suggested that several misincorporations of a single nucleotide occurred without deletions or additions. In addition, these results were consistent with the hypothesis that a correct incorporation among multiple misincorporations facilitated the strand-displacement activity of tPolλ.

DISCUSSION

Mechanistic Studies of DNA Polymerization. In this paper, we overexpressed and purified the polβ-like domain of Polλ (tPolλ) (Figure 1). In our limited mechanistic studies of tPolλ, we determined the dNTP dissociation rate constant of 300 s^{-1} by performing an unlabeled dGTP trapping experiment (Figure 3 inset). As far as we know, this is the first direct measurement of the dissociation rate constant of a nucleotide from the ground-state ternary complex E·DNA·dNTP. However, this ground-state complex may not form in the absence of Mg^{2+} on the basis of published crystal structures and metal ion binding studies of other polymerases (*42*−*44*). These studies have revealed a common two-metal-ion catalytic mechanism: one divalent ion is involved in both positioning the α-phosphate of the incoming nucleotide and activation of its 3′-hydroxyl group as a nucleophile; the other metal ion both anchors the binding of the β- and γ-phosphates of the nucleotide and assists the leaving of the pyrophosphate. The small amount of radiolabeled product shown in Figure 3 (inset) suggested the existence of E·DNA·dNTP. However, we cannot exclude the possibility that this complex may not be the same complex in the absence and presence of Mg^{2+}. Furthermore, the measured dissociation rate constant should not be for the nucleotide dissociation from the tight binding ternary complex E′·DNA·dNTP which formed after the initial

E·DNA·dNTP complex undergoes protein conformational change. This is because the binding of the divalent metal ions induces the protein conformational change which may be a prerequisite for catalytic activity by correctly positioning the side chains of the residues located at the polymerase active site (*35*, *45*). Moreover, the measured dissociation rate constant (300 s^{-1}) is too high for nucleotide dissociation from the tight binding ternary complex E′·DNA·dNTP. The nucleotide association rate constant (1.55×10^8 M^{-1} s^{-1}) calculated from this nucleotide dissociation rate constant also supports the measured dissociation rate constant to be for nucleotide dissociation from the ternary complex E·DNA·dNTP since a small nucleotide molecule is expected to bind to the E·DNA binary complex at a rate constant close to the diffusion limit (1.0×10^8 M^{-1} s^{-1}). The large nucleotide association and dissociation rate constants indicated a rapid equilibrium of nucleotide binding relative to nucleotide incorporation.

In the absence of the unlabeled dGTP trap, the incorporation of [α-^{32}P]dGTP allowed us to measure the DNA dissociation rate constant of 0.8 s^{-1}, which was less than 3-fold lower than the nucleotide incorporation rate constant (Figure 3). This suggested tPolλ has a processivity [$= k_p/(k_1 + k_p)$] of 0.72, which is defined as the likelihood of incorporating the next correct nucleotide following each correct nucleotide incorporation event. The processivity value of a highly processive DNA polymerase is close to 1 due to k_p being much larger than k_1. However, the processivity of tPolλ is low, which is consistent with previous reports suggesting that this enzyme is not a processive polymerase (*10*, *13*, *17*) and with its potential function as a polymerase which fills short-patched DNA gaps in base excision repair pathways (see discussion below). The fast DNA dissociation rate constant has also been found with Polβ (*41*).

The proposed kinetic mechanism shown in Scheme 1 can explain all of our kinetic data at present. However, it is a minimal mechanism and requires more studies to be completed. For example, the nucleotide incorporation in the first turnover could be limited by either a putative protein conformational change, as observed in replicative DNA polymerases such as T7 DNA polymerase (*34*) and human mitochondrial DNA polymerase (*39*) and in Y-family DNA polymerases such as yeast DNA polymerase η (*33*) and *S. solfataricus* P2 DNA polymerase IV (*32*), or the chemistry step, as observed only in the X-family DNA polymerase Polβ (*44*, *46*). It would be interesting to see if the chemistry step is also rate-limiting in the first turnover of nucleotide incorporation catalyzed by another X-family polymerase tPolλ. The detailed kinetic mechanism of tPolλ is currently being studied in our laboratory.

Fidelity of DNA Polymerization. The construct of tPolλ, unlike the full-length Polλ, did not exhibit dNTP substrate inhibition in our kinetic experiments (Figures 4 and 5), which allowed us to estimate the fidelity of the full-length Polλ using pre-steady-state kinetic assays. The N-terminal BRCT and proline-rich domains (Figure 1A) could affect the misincorporation fidelity by the full-length Polλ. However, the fidelity of nucleotide incorporation into D-1 by the full-length Polλ was measured to be in the range of $10^{-3}-10^{-4}$ (data not shown) which is similar to the fidelity of tPolλ (Table 2). Thus, the N-terminal domains do not affect the intrinsic fidelity of Polλ although they either mediate the protein/protein or protein/DNA interactions through the BRCT domain or regulate the polymerase activity of Polλ through the proline-rich domain (*10*−*13*). This hypothesis is supported by the preliminary results that dNTP substrate inhibition was only observed with the full-length Polλ, not tPolλ.

Under single turnover conditions, the fidelity of tPolλ was estimated to be 3.2×10^{-2} for the T·dGMP misincorporation and $10^{-3}-10^{-4}$ for all other incorrect incorporations (Table 2). The latter value is similar to the single base substitution error rate of 9.0×10^{-4} when Polλ fills a 5′-nucleotide gap at a TGA codon in the *lacZ* gene in M13mp2 DNA (*13*). It is also similar to the base substitution rate of Polλ (9.0×10^{-4}) scored both in the *lacZ* α gene in M13mp2 during synthesis to fill a 407-nucleotide gap and in the 6-nucleotide gap frame-shift reversion assay (*22*). Interestingly, these M13mp2-based assays (*13*, *22*) also reveal that the substitution error is 10-fold higher at the T·dGMP wobble base pair than other mispairs. This observation agrees with our kinetic results (Table 2). Therefore, the results from these M13mp2-based assays are consistent with the results generated from our pre-steady-state kinetic analysis. However, only our analysis revealed the kinetic basis for the fidelity of Polλ: (i) the selection was predominantly from the 10−1000-fold difference in incorporation rates of correct and incorrect nucleotides while the ground-state binding affinity provided only about a 2-fold contribution, and (ii) the 10-fold lower fidelity at the wobble T·dGMP base pair is mainly due to the 10−100-fold higher misincorporation rate compared to the other mispairs (Table 2). Notably, we did not observe any frame shifts which have been found to be extremely high ($10^{-2}-10^{-3}$) by the M13mp2-based assays (*22*). This difference can probably be attributed to different DNA gap sizes: we used a single-nucleotide gap in our studies while K. Bebenek et al. used either 6- or 407-nucleotide gaps. The downstream 5′-phosphorylated primer 19-mer in our DNA substrate 21-19/41-mer formed base pairs with the template 41-mer and prevented the formation of a misaligned frame-shift DNA intermediate since only one template base was not paired. The weak strand-displacement activity of tPolλ (see below) should not affect the frame-shift frequency since this activity each time unwinded only one base pair formed between the 19-mer and 41-mer when a single-nucleotide gap is filled.

The fidelity of tPolλ is about 10−100-fold lower than the fidelity of rat Polβ (recalculated as $10^{-4}-10^{-5}$ using the definition of fidelity in Table 2) which was measured under single turnover conditions with a single-nucleotide gapped DNA 25-19/45-mer (primer-primer/template) (*41*). A 5−10-fold higher substitution rate of Polλ over Polβ was also observed by the M13mp2-based assays (*22*). Interestingly, the unusually high infidelity for the wobble T·dGMP misincorporation was not observed with Polβ (*41*). In Polβ, the nucleotide ground-state binding affinity contributes 10−100-fold to the fidelity in addition to the 100−1000-fold contribution from the incorporation rates (*41*). The higher selection in the nucleotide ground-state binding step thereby contributes to higher fidelity of Polβ over Polλ. The incorporation rates for both correct and incorrect nucleotides are faster with Polβ than with tPolλ. The binding affinity of correct nucleotides to these two polymerases is similarly high, but the incorrect nucleotides are more weakly bound

Table 3: Different Kinetic Parameters of Human DNA tPolλ and Rat DNA Polβ in the Presence of A Single-Nucleotide Gapped DNA Substrate

	tPolλ		Polβ[a]	
	correct	incorrect	correct	incorrect
K_d (μM)	1.1−2.4	1.4−8.4	1.9−8.5	190−1600
k_p (s^{-1})	3.0−6.0	0.001−0.20	12−36	0.019−1.3
k_p/K_d ($\mu M^{-1} s^{-1}$)	2.1−2.7	(2.8−710) × 10^{-4}	4−6	(7−250) × 10^{-5}
fidelity[b]	10^{-2}−10^{-4}		10^{-4}−10^{-5}	

[a] Reference *24*. [b] Calculated as $(k_p/K_d)_{incorrect}/[(k_p/K_d)_{correct} + (k_p/K_d)_{incorrect}]$.

by Polβ than by tPolλ (see below). These results suggest that Polβ and Polλ are quite different enzymes although they share sequence homology and are expected to have structural similarity (*10*−*13*). These different enzyme activities lead us to believe that these two polymerases play different biological roles.

Wobble T·dGMP Base Pair. Although the ground-state binding affinity is similar, Table 2 shows that the misincorporation rate of dGTP opposite template base T is only about 10-fold slower than the incorporation of correct dATP and is much faster than all other misincoporations including dTTP opposite template base G. Such an asymmetry between T·dGMP and G·dTMP has been observed with DNA polymerase ι (*47*) and not with any other DNA polymerases including replicative polymerases. In DNA polymerase ι, the values of the substrate specificity estimated by steady-state kinetic analysis are 1.5 × 10^{-1} and 2.85 × 10^{-2} for the incorporations of T·dGMP and G·dTMP, respectively (*47*). The incorporation efficiency difference is even larger (11-fold) with tPolλ (Table 2). It would be interesting to see if such an asymmetry also occurs to the full-length Polλ. The reason for the faster formation of the T·dGMP wobble base pair over the G·dTMP is not clear and cannot be explained simply from a hydrogen-bonding perspective. It could be rationalized by consideration of increasingly favorable base-stacking interactions between dGTP, a purine, with the 3′-end base of the primer over a pyrimidine like dTTP. The more stabilized T·dGMP, when compared to G·dTMP, could align the 3′-hydroxyl moiety of the primer and the incoming nucleotide more favorably at the enzyme active site and facilitate catalysis. The reason for the faster formation of the T·dGMP wobble base pair over the other 10 mispairs is not clear either. It could be rationalized by more hydrogen bonds between bases G and T than other mispairs. Interestingly, the asymmetry between the incorporations of T·dGMP and G·dTMP is not observed with Polβ (*41*), suggesting that the active sites of the two X-family members are different. Further studies are needed to resolve the structural basis of this wobble base pair in terms of which amino acid residues and what type of interactions are involved in the T·dGMP wobble base pairing.

Tight Ground-State Binding of the Incoming Nucleotide. It is not surprising that the correct nucleotides are incorporated by tPolλ much faster than the incorrect nucleotides. However, Table 2 shows that the incoming nucleotides, regardless of whether they are correct or incorrect, have relatively high and peculiarly similar binding affinity to the binary complex of tPolλ and the single-nucleotide gapped DNA substrate. The tight binding of all incorrect nucleotides is unprecedented since most of DNA polymerases which have been studied so far generally discriminate against incorrect nucleotides by binding them weakly and incorporating them slowly (*48*). For example, the mismatched nucleotides have 100−200-fold weaker binding affinity than the matched ones to the binary complex of Polβ and a single-nucleotide gapped DNA (Table 3) (*41*). The only exception is the binding affinity of mismatched dGTP opposite a template base G in a single-nucleotide gapped DNA substrate by African swine fever virus polymerase X, which is 5-fold tighter than the Watson−Crick base pair dCTP·G (*49*). Interestingly, this enzyme is another member of the X-family DNA polymerases. The tighter binding of mismatched dGTP over matched dCTP is probably because this X-family polymerase has higher intrinsic affinity toward deoxypurine triphosphates than deoxypyrimidine triphosphates (*50*−*52*).

The tight binding of matched nucleotides by Polβ with the gapped DNA is partly due to the contribution of its 8 kDa dRPase domain revealed by crystal structures (*48*). This domain does not specifically contact the DNA, nucleotide, nor the rest of Polβ in the presence of a nongapped DNA substrate (*9*) but shows intense interactions with the downstream primer and the 31 kDa domain in the presence of a single-nucleotide gapped DNA (*53*). This leads to tighter interactions between the incoming nucleotide and surrounding amino acid residues. Although unavailable at present, modeling studies show that the ternary structure of tPolλ is expected to be similar to the structure of Polβ and the tight binding of the correct nucleotide by tPolλ is thus structurally reasonable. However, the difference in the binding affinity of incorrect nucleotides by the two homologous X-family members is significant (Table 3). Although the residues surrounding the incoming nucleotide in Polβ are mostly conserved in Polλ, sequence alignment analysis suggests the residues K27, R40, A185, K280, and D276 in human Polβ are changed to S268, A280, K422, R514, and A510 in human Polλ, respectively (*13*, *22*). Residue D276, which makes van der Waals interactions with the base of the incoming nucleotide in Polβ (*53*), weakens nucleotide binding due to its negative charge. Mutation of this residue to a neutral residue (e.g., valine and glycine) increases the correct nucleotide binding affinity by 4−9-fold and incorrect nucleotide binding affinity by 2.5-fold (*48*, *54*). Consequently, its replacement with the uncharged A510 in Polλ could account for the increase in the nucleotide binding affinity, particularly for incorrect nucleotides. We are currently studying the roles of A510 and the other four residues in the binding of nucleotides by tPolλ through site-directed mutagenesis and single turnover kinetic assays.

Weak Strand-Displacement Activity. Multiple product formation patterns shown in Figure 6 suggest that the downstream base pairs formed between the 19-mer primer and the 41-mer template were melted during polymerization.

The melting could be due to either thermal breathing of the 5′-terminus of the 19-mer or the strand-displacement activity of tPolλ or both. Interestingly, the misincorporations of dCTP into D-1, D-7, and D-8 and the misincorporation of dTTP into D-12 yielded longer products than other types of mismatches, and the values of substrate specificity were slightly higher (Table 2). These observations suggest that the strand-displacement activity of tPolλ, rather than thermal breathing, was the major force to melt downstream base pairs during polymerization. Such an activity of tPolλ has been observed previously (*14*). The energy source for this weak strand-displacement activity is probably derived from the net favorable free energy of nucleotide incorporation. One matched incorporation among multiple misincorporations (G•dCMP in D-1, D-7, and D-8; A•dTMP in D-12) facilitates the strand-displacement activity of tPolλ since the net favorable energy yielded from a correct nucleotide incorporation will be larger than from the incorporation of a mismatched nucleotide.

Potential Biological Functions. Polλ has been suggested to play a role in DNA repair synthesis associated with meiosis since it is found to be predominantly expressed in testis in stages of spermatogenesis (*11*). Polλ does not have a proof-reading exonuclease function but possesses a dRPase and strand-displacement activity (Figure 6). Moreover, Polλ has a BRCT domain which mediates protein/protein and protein/DNA interactions. Therefore, Polλ has been proposed to play a similar role as Polβ in BER (*14*). Since the insertion fidelity of full-length Polλ was as low as the fidelity of tPolλ (10^{-2}−10^{-4}) on the basis of our preliminary studies, the error rate will be too high for Polλ to function as the DNA polymerase in long-patch BER proposed previously (*14*, *19*). However, Polλ, like Polβ, could function as a DNA polymerase in "short-patch" BER since the mutation possibility will be minimized if it only incorporates one nucleotide in a single-nucleotide gap. This potential function is indirectly supported by the high frame-shift rate of Polλ as revealed by both the forward mutation assay (*22*) and the short-gap frame-shift reversion assay (*13*). The high frame-shift rate would be detrimental to genetic stability if the polymerase makes a lot of deletions when it fills a large DNA gap. In addition, the low processivity (see above discussion) and weak strand-displacement activity of Polλ also support its role in short-patch BER, rather than long-patch BER.

Recent immunodepletion studies reveal that Polλ is the primary DNA polymerase to fill one- or two-nucleotide gaps during NHEJ in an *in vitro* system based on human nuclear extracts and that the BRCT domain of Polλ is required for this short-gap filling activity (*23*). The low fidelity and short-gap filling ability of Polλ revealed by our studies support this potential role. Moreover, we and others (*13*, *17*) have observed the dNTP substrate inhibition with the full-length Polλ. These observations, coupled with the tight binding of nucleotides (Table 2), suggest that Polλ would function as a polymerase at low cellular concentrations of dNTPs. Interestingly, cellular dNTP concentrations are highest during S and G_2 phases and lowest during the G_0 phase (*55*), and the NHEJ pathway plays a dominant role in repairing γ-radiation-induced DSBs during G_0, G_1, and early S phases while homologous recombination is preferentially used in late S and G_2 phases (*56*). These results support the hypothesis that Polλ may function as a polymerase in the NHEJ pathway during the G_0 phase (*18*, *22*, *23*). This potential function is further substantiated by the end-joining role of its close homologue in yeast, DNA polymerase IV (*57*, *58*).

ACKNOWLEDGMENT

We thank Sudarshan Seshadri for helping us to subclone and purify tPolλ.

REFERENCES

1. Lindahl, T. (1993) Instability and decay of the primary structure of DNA, *Nature 362*, 709−715.
2. Burgers, P. M. (1998) Eukaryotic DNA polymerases in DNA replication and DNA repair, *Chromosoma. 107*, 218−227.
3. Klungland, A., and Lindahl, T. (1997) Second pathway for completion of human DNA base excision-repair: reconstitution with purified proteins and requirement for DNase IV (FEN1), *EMBO J. 16*, 3341−3348.
4. Frosina, G., Fortini, P., Rossi, O., Carrozzino, F., Raspaglio, G., Cox, L. S., Lane, D. P., Abbondandolo, A., and Dogliotti, E. (1996) Two pathways for base excision repair in mammalian cells, *J. Biol. Chem. 271*, 9573−9578.
5. Wilson, S. H. (1998) Mammalian base excision repair and DNA polymerase beta, *Mutat. Res. 407*, 203−215.
6. Beard, W. A., and Wilson, S. H. (2000) Structural design of a eukaryotic DNA repair polymerase: DNA polymerase beta, *Mutat. Res. 460*, 231−244.
7. Matsumoto, Y., and Kim, K. (1995) Excision of deoxyribose phosphate residues by DNA polymerase beta during DNA repair, *Science 269*, 699−702.
8. Podlutsky, A. J., Dianova, II, Wilson, S. H., Bohr, V. A., and Dianov, G. L. (2001) DNA synthesis and dRPase activities of polymerase beta are both essential for single-nucleotide patch base excision repair in mammalian cell extracts, *Biochemistry 40*, 809−813.
9. Pelletier, H., Sawaya, M. R., Kumar, A., Wilson, S. H., and Kraut, J. (1994) Structures of ternary complexes of rat DNA polymerase beta, a DNA template-primer, and ddCTP, *Science 264*, 1891−1903.
10. Aoufouchi, S., Flatter, E., Dahan, A., Faili, A., Bertocci, B., Storck, S., Delbos, F., Cocea, L., Gupta, N., Weill, J. C., and Reynaud, C. A. (2000) Two novel human and mouse DNA polymerases of the polX family, *Nucleic Acids Res. 28*, 3684−3693.
11. Garcia-Diaz, M., Dominguez, O., Lopez-Fernandez, L. A., de Lera, L. T., Saniger, M. L., Ruiz, J. F., Parraga, M., Garcia-Ortiz, M. J., Kirchhoff, T., del Mazo, J., Bernad, A., and Blanco, L. (2000) DNA polymerase lambda (Pol lambda), a novel eukaryotic DNA polymerase with a potential role in meiosis, *J. Mol. Biol. 301*, 851−867.
12. Nagasawa, K., Kitamura, K., Yasui, A., Nimura, Y., Ikeda, K., Hirai, M., Matsukage, A., and Nakanishi, M. (2000) Identification and characterization of human DNA polymerase beta 2, a DNA polymerase beta -related enzyme, *J. Biol. Chem. 275*, 31233−31238.
13. Garcia-Diaz, M., Bebenek, K., Sabariegos, R., Dominguez, O., Rodriguez, J., Kirchhoff, T., Garcia-Palomero, E., Picher, A. J., Juarez, R., Ruiz, J. F., Kunkel, T. A., and Blanco, L. (2002) DNA polymerase lambda, a novel DNA repair enzyme in human cells, *J. Biol. Chem. 277*, 13184−13191.
14. Garcia-Diaz, M., Bebenek, K., Kunkel, T. A., and Blanco, L. (2001) Identification of an intrinsic 5′-deoxyribose-5-phosphate lyase activity in human DNA polymerase lambda: a possible role in base excision repair, *J. Biol. Chem. 276*, 34659−34663.
15. DeRose, E. F., Kirby, T. W., Mueller, G. A., Bebenek, K., Garcia-Diaz, M., Blanco, L., Kunkel, T. A., and London, R. E. (2003) Solution structure of the lyase domain of human DNA polymerase lambda, *Biochemistry 42*, 9564−9574.
16. Bork, P., Hofmann, K., Bucher, P., Neuwald, A. F., Altschul, S. F., and Koonin, E. V. (1997) A superfamily of conserved domains in DNA damage-responsive cell cycle checkpoint proteins, *FASEB J. 11*, 68−76.
17. Shimazaki, N., Yoshida, K., Kobayashi, T., Toji, S., Tamai, K., and Koiwai, O. (2002) Overexpression of human DNA polymerase lambda in E. coli and characterization of the recombinant enzyme, *Genes Cells 7*, 639−651.

18. Ramadan, K., Maga, G., Shevelev, I. V., Villani, G., Blanco, L., and Hubscher, U. (2003) Human DNA polymerase lambda possesses terminal deoxyribonucleotidyl transferase activity and can elongate RNA primers: implications for novel functions, *J. Mol. Biol. 328*, 63−72.
19. Ramadan, K., Shevelev, I. V., Maga, G., and Hubscher, U. (2002) DNA polymerase lambda from calf thymus preferentially replicates damaged DNA, *J. Biol. Chem. 277*, 18454−18458.
20. Maga, G., Villani, G., Ramadan, K., Shevelev, I., Tanguy Le Gac, N., Blanco, L., Blanca, G., Spadari, S., and Hubscher, U. (2002) Human DNA polymerase lambda functionally and physically interacts with proliferating cell nuclear antigen in normal and translesion DNA synthesis, *J. Biol. Chem. 277*, 48434−48440.
21. Kobayashi, Y., Watanabe, M., Okada, Y., Sawa, H., Takai, H., Nakanishi, M., Kawase, Y., Suzuki, H., Nagashima, K., Ikeda, K., and Motoyama, N. (2002) Hydrocephalus, situs inversus, chronic sinusitis, and male infertility in DNA polymerase lambda-deficient mice: possible implication for the pathogenesis of immotile cilia syndrome, *Mol. Cell. Biol. 22*, 2769−2776.
22. Bebenek, K., Garcia-Diaz, M., Blanco, L., and Kunkel, T. A. (2003) The frameshift infidelity of human DNA polymerase lambda. Implications for function, *J. Biol. Chem. 278*, 34685−34690.
23. Lee, J. W., Blanco, L., Zhou, T., Garcia-Diaz, M., Bebenek, K., Kunkel, T. A., Wang, Z., and Povirk, L. F. (2004) Implication of DNA polymerase lambda in alignment-based gap filling for nonhomologous DNA end joining in human nuclear extracts, *J. Biol. Chem. 279*, 805−811.
24. Ahn, J., Werneburg, B. G., and Tsai, M. D. (1997) DNA polymerase beta: structure-fidelity relationship from Pre-steady-state kinetic analyses of all possible correct and incorrect base pairs for wild type and R283A mutant, *Biochemistry 36*, 1100−1107.
25. Gutfreund, H. (1972) *Enzymes: Physical Principles*, Wiley-Interscience, New York.
26. Johnson, K. A. (1992) Transient-state kinetic analysis of enzyme reaction pathways, *Enzymes 20*, 1−61.
27. Suo, Z., Lippard, S. J., and Johnson, K. A. (1999) Single d(GpG)/cis-diammineplatinum(II) adduct-induced inhibition of DNA polymerization, *Biochemistry 38*, 715−726.
28. Suo, Z., and Johnson, K. A. (1997) Effect of RNA secondary structure on the kinetics of DNA synthesis catalyzed by HIV-1 reverse transcriptase, *Biochemistry 36*, 12459−12467.
29. Suo, Z., and Johnson, K. A. (1998) DNA secondary structure effects on DNA synthesis catalyzed by HIV-1 reverse transcriptase, *J. Biol. Chem. 273*, 27259−27267.
30. Liu, J., and Tsai, M. D. (2001) DNA polymerase beta: pre-steady-state kinetic analyses of dATP alpha S stereoselectivity and alteration of the stereoselectivity by various metal ions and by site-directed mutagenesis, *Biochemistry 40*, 9014−9022.
31. Fiala, K. A., and Suo, Z. (2004) Pre-Steady-State Kinetic Studies of the Fidelity of *Sulfolobus solfataricus* P2 DNA Polymerase IV, *Biochemistry 43*, 2106−2115.
32. Fiala, K. A., and Suo, Z. (2004) Mechanism of DNA Polymerization Catalyzed by *Sulfolobus solfataricus* P2 DNA Polymerase IV, *Biochemistry 43*, 2116−2125.
33. Washington, M. T., Prakash, L., and Prakash, S. (2001) Yeast DNA polymerase eta utilizes an induced-fit mechanism of nucleotide incorporation, *Cell 107*, 917−927.
34. Patel, S. S., Wong, I., and Johnson, K. A. (1991) Pre-steady-state kinetic analysis of processive DNA replication including complete characterization of an exonuclease-deficient mutant, *Biochemistry 30*, 511−525.
35. Zhong, X., Patel, S. S., Werneburg, B. G., and Tsai, M. D. (1997) DNA polymerase beta: multiple conformational changes in the mechanism of catalysis, *Biochemistry 36*, 11891−11900.
36. Dahlberg, M. E., and Benkovic, S. J. (1991) Kinetic mechanism of DNA polymerase I (Klenow fragment): identification of a second conformational change and evaluation of the internal equilibrium constant, *Biochemistry 30*, 4835−4843.
37. Bryant, F. R., Johnson, K. A., and Benkovic, S. J. (1983) Elementary steps in the DNA polymerase I reaction pathway, *Biochemistry 22*, 3537−3546.
38. Kuchta, R. D., Benkovic, P., and Benkovic, S. J. (1988) Kinetic mechanism whereby DNA polymerase I (Klenow) replicates DNA with high fidelity, *Biochemistry 27*, 6716−6725.
39. Johnson, A. A., Tsai, Y., Graves, S. W., and Johnson, K. A. (2000) Human mitochondrial DNA polymerase holoenzyme: reconstitution and characterization, *Biochemistry 39*, 1702−1708.
40. Eger, B. T., Kuchta, R. D., Carroll, S. S., Benkovic, P. A., Dahlberg, M. E., Joyce, C. M., and Benkovic, S. J. (1991) Mechanism of DNA replication fidelity for three mutants of DNA polymerase I: Klenow fragment KF(exo+), KF(polA5), and KF(exo-), *Biochemistry 30*, 1441−1448.
41. Ahn, J., Kraynov, V. S., Zhong, X., Werneburg, B. G., and Tsai, M. D. (1998) DNA polymerase beta: effects of gapped DNA substrates on dNTP specificity, fidelity, processivity and conformational changes, *Biochem. J. 331* (Part 1), 79−87.
42. Steitz, T. A. (1998) A mechanism for all polymerases, *Nature 391*, 231−232.
43. Steitz, T. A. (1999) DNA polymerases: structural diversity and common mechanisms, *J. Biol. Chem. 274*, 17395−17398.
44. Arndt, J. W., Gong, W., Zhong, X., Showalter, A. K., Liu, J., Dunlap, C. A., Lin, Z., Paxson, C., Tsai, M. D., and Chan, M. K. (2001) Insight into the catalytic mechanism of DNA polymerase beta: structures of intermediate complexes, *Biochemistry 40*, 5368−5375.
45. Bougie, I., Charpentier, S., and Bisaillon, M. (2003) Characterization of the metal ion binding properties of the hepatitis C virus RNA polymerase, *J. Biol. Chem. 278*, 3868−3875.
46. Dunlap, C. A., and Tsai, M. D. (2002) Use of 2-aminopurine and tryptophan fluorescence as probes in kinetic analyses of DNA polymerase beta, *Biochemistry 41*, 11226−11235.
47. Zhang, Y., Yuan, F., Wu, X., and Wang, Z. (2000) Preferential incorporation of G opposite template T by the low-fidelity human DNA polymerase iota, *Mol. Cell. Biol. 20*, 7099−7108.
48. Vande Berg, B. J., Beard, W. A., and Wilson, S. H. (2001) DNA structure and aspartate 276 influence nucleotide binding to human DNA polymerase beta. Implication for the identity of the rate-limiting conformational change, *J. Biol. Chem. 276*, 3408−3416.
49. Showalter, A. K., and Tsai, M. D. (2001) A DNA polymerase with specificity for five base pairs, *J. Am. Chem. Soc. 123*, 1776−1777.
50. Beard, W. A., and Wilson, S. H. (2001) DNA polymerases lose their grip, *Nat. Struct. Biol. 8*, 915−917.
51. Maciejewski, M. W., Shin, R., Pan, B., Marintchev, A., Denninger, A., Mullen, M. A., Chen, K., Gryk, M. R., and Mullen, G. P. (2001) Solution structure of a viral DNA repair polymerase, *Nat. Struct. Biol. 8*, 936−941.
52. Showalter, A. K., Byeon, I. J., Su, M. I., and Tsai, M. D. (2001) Solution structure of a viral DNA polymerase X and evidence for a mutagenic function, *Nat. Struct. Biol. 8*, 942−946.
53. Sawaya, M. R., Prasad, R., Wilson, S. H., Kraut, J., and Pelletier, H. (1997) Crystal structures of human DNA polymerase beta complexed with gapped and nicked DNA: evidence for an induced fit mechanism, *Biochemistry 36*, 11205−11215.
54. Lavrik, O. I., Prasad, R., Beard, W. A., Safronov, I. V., Dobrikov, M. I., Srivastava, D. K., Shishkin, G. V., Wood, T. G., and Wilson, S. H. (1996) dNTP binding to HIV-1 reverse transcriptase and mammalian DNA polymerase beta as revealed by affinity labeling with a photoreactive dNTP analog, *J. Biol. Chem. 271*, 21891−21897.
55. Reichard, P. (1988) Interactions between deoxyribonucleotide and DNA synthesis, *Annu. Rev. Biochem. 57*, 349−374.
56. Takata, M., Sasaki, M. S., Sonoda, E., Morrison, C., Hashimoto, M., Utsumi, H., Yamaguchi-Iwai, Y., Shinohara, A., and Takeda, S. (1998) Homologous recombination and non-homologous end-joining pathways of DNA double-strand break repair have overlapping roles in the maintenance of chromosomal integrity in vertebrate cells, *EMBO J. 17*, 5497−5508.
57. Wilson, T. E., and Lieber, M. R. (1999) Efficient processing of DNA ends during yeast nonhomologous end joining. Evidence for a DNA polymerase beta (Pol4)-dependent pathway, *J. Biol. Chem. 274*, 23599−23609.
58. Tseng, H. M., and Tomkinson, A. E. (2002) A physical and functional interaction between yeast Pol4 and Dnl4-Lif1 links DNA synthesis and ligation in nonhomologous end joining, *J. Biol. Chem. 277*, 45630−45637.

BI049975C